

## TEMPLATE ROTATION CURVES FOR DISK GALAXIES

BARBARA CATINELLA<sup>1</sup>, RICCARDO GIOVANELLI<sup>2</sup>, & MARTHA P. HAYNES<sup>2</sup>*Accepted for publication in the Astrophysical Journal*

## ABSTRACT

A homogeneous sample of  $\sim 2200$  low redshift disk galaxies with both high sensitivity long-slit optical spectroscopy and detailed *I*-band photometry is used to construct average, or template, rotation curves in separate luminosity classes, spanning 6 magnitudes in *I*-band luminosity. The template rotation curves are expressed as functions both of exponential disk scale lengths  $r_d$  and of optical radii  $R_{\text{opt}}$ , and extend out to 4.5–6.5  $r_d$ , depending on the luminosity bin. The two parameterizations yield slightly different results beyond  $R_{\text{opt}}$  because galaxies whose H $\alpha$  emission can be traced to larger extents in the disks are typically of higher optical surface brightness and are characterized by larger values of  $R_{\text{opt}}/r_d$ . By either parameterization, these template rotation curves show no convincing evidence of velocity decline within the spatial scales over which they are sampled, even in the case of the most luminous systems. In contrast to some previous expectations, the fastest rotators (most luminous galaxies) have, on average, rotation curves that are flat or mildly rising beyond the optical radius, implying that the dark matter halo makes an important contribution to the kinematics also in these systems. The template rotation curves and the derived functional fits provide quantitative constraints for studies of the structure and evolution of disk galaxies, which aim at reproducing the internal kinematics properties of disks at the present cosmological epoch.

*Subject headings:* galaxies: kinematics and dynamics — galaxies: spiral — galaxies: structure — cosmology: observations — dark matter

## 1. INTRODUCTION

The determination of the rotational characteristics of galaxy disks is fundamental to understanding the role that dynamics plays in galaxy formation and evolution over cosmic time. Over the last decade, a large number of studies have addressed the issue of disk formation and evolution in current hierarchical cosmologies by means of analytical or semi-analytical theoretical models (e.g., Dalcanton, Spergel, & Summers 1997; Mo, Mao, & White 1998; Mao, Mo, & White 1998; Mo & Mao 2004; Avila-Reese, Firmani, & Hernández 1998; Firmani & Avila-Reese 2000; van den Bosch 2001, 2002) and numerical smooth particle hydrodynamic simulations (e.g., van den Bosch et al. 2002; Abadi et al. 2003; Governato et al. 2004). Other groups have investigated more specifically the characteristics of the density profiles of dark matter halos, which directly determine the observable rotation curves (RCs) of present-day disks, using *N*-body simulations (e.g., Navarro, Frenk, & White 1996, 1997; Bullock et al. 2001a,b). A detailed characterization of the kinematic properties of observed disk galaxies at low redshift is of key importance to validate such models and place constraints on the properties of dark matter halos. In this context, special attention has been recently devoted to dwarf and low surface brightness galaxies, i.e. systems with an internal kinematics that is thought to be dominated by dark matter even at small radii, thus allowing

to best probe the inner structure of their parent halos (e.g., Spekkens, Giovanelli, & Haynes 2005 and references therein). For high surface brightness galaxies, the kinematics is easier to measure, but the presence of a more prominent stellar disk complicates the analysis of the RC, whose decomposition into a dark matter and a disk component is generally not unique (see, for instance, Jimenez, Verde, & Oh 2003; Dutton et al. 2005, and references therein).

The derivation of *average* RCs representative of the kinematic properties of a large number of local spirals is also important on its own, to provide a standard reference against which similar, distant samples can be compared. Furthermore, statistical descriptors of the amplitude and radial variation of rotation velocity within disks would benefit all the applications that rely on the assumption of a RC model, such as determinations of rotational widths from spectroscopic data that lack velocity or spatial resolution. Examples of the latter include internal kinematic studies of intermediate redshift spirals through spatially resolved optical spectroscopy, where synthetic RCs are needed in order to estimate the full velocity width (e.g., Vogt et al. 1997; Simard & Pritchett 1999; Ziegler et al. 2003; Böhm et al. 2004).

Beginning perhaps with Roberts & Rots (1973), many previous works have explored the variation in rotation curve form among galaxies. As larger samples of rotation curves have been amassed, attempts have been made to produce more quantitative descriptions of empirically-derived average, or *template* RCs. Notably, average RCs binned by luminosity and with radial distances expressed in units of the optical radius  $R_{\text{opt}}$  defined as the radius encompassing 83% of the total integrated light were previously presented by Persic, Salucci, & Stel (1996, hereafter PSS96) for a sample of 616 spiral galaxies. This definition of  $R_{\text{opt}}$  is equivalent to  $3.2 r_d$  for a pure ex-

<sup>1</sup> National Astronomy and Ionosphere Center, Arecibo Observatory, HC3 Box 53995, Arecibo, PR 00612, USA; bcatinel@naic.edu. The National Astronomy and Ionosphere Center is operated by Cornell University under a cooperative agreement with the National Science Foundation.

<sup>2</sup> Center for Radiophysics and Space Research and National Astronomy and Ionosphere Center, Cornell University, Ithaca, NY 14853, USA; riccardo@astro.cornell.edu, haynes@astro.cornell.edu.

ponential disk. PSS96 showed that their average RCs were well described by an analytical form, obtained as the combination in quadrature of a dark matter halo and an exponential disk, with fit coefficients depending on galaxy luminosity only. Based on these results they claimed the existence of a universal relation, the *universal rotation curve* (URC), whereby the shape and amplitude of an *observed* RC at any radius is completely determined by the galaxy luminosity, as originally proposed by Persic & Salucci (1991). According to the URC predictions, the most luminous systems have RCs that peak at  $\sim 0.8 R_{\text{opt}}$  and decline beyond that radius, implying a minor contribution of the dark matter halos to the internal kinematics of those galaxies. It should be also noticed, however, that PSS96's average RC tracings beyond  $R_{\text{opt}}$  are based on linear extrapolations of outer velocity gradients as functions of luminosity mostly obtained from H I data. Several studies have discussed the inadequacy of the URC parameterization (e.g., Courteau 1997; Verheijen 1997; Willick 1999; Garrido, Marcellin & Amram 2004).

The purpose of this paper is to provide a set of template RCs in bins covering a wide range of galaxy luminosity and based on an extensive set of high sensitivity long-slit optical RCs, for which a homogeneous body of high quality *I*-band photometry is also available. Our intent is not to propose a new universal relation, but rather to obtain a more reliable characterization of the average RCs of late type, high brightness disk galaxies by taking advantage of a much larger data set, thereby negating the need for extrapolation within the optical disk. In order to allow a direct comparison with PSS96's average RCs and URC models, we provide template RCs parameterized as functions of  $R_{\text{opt}}$ . Furthermore, we also present a set of templates which parameterize the distance from the center of a galaxy by means of the exponential disk scale length  $r_d$ , a quantity naturally adopted in models of galaxy disks.

This work makes use of a large spiral galaxy photometric and spectroscopic dataset, dubbed SFI++ (see § 2), compiled to investigate the internal kinematics of disk galaxies at low redshifts, as well as to study the peculiar velocity field in the local universe via application of the Tully-Fisher (TF; Tully & Fisher 1977) method. Details on the extraction of related quantities from long-slit spectra, including our RC folding technique and algorithm for the measurement of rotational velocities for TF applications, can be found in Catinella, Haynes, & Giovanelli (2005, hereafter CHG05).

This paper is organized as follows. In § 2 we describe our data sample and illustrate the procedure used to derive template RCs. The results obtained using the parameterizations in terms of exponential disk scale lengths or optical radii are presented and compared in § 3. In order to explain systematic differences between the outer slopes of the two sets of template RCs, the correlation between  $R_{\text{opt}}/r_d$  ratio and RC extent observed for the galaxies in our sample is also investigated in some detail. The impact of internal extinction on the inner slopes of RCs is analyzed in § 4, where template RCs are computed for separate intervals of galaxy inclination. The comparison with previously published results, most notably the URC models, is discussed in § 5, and our conclusions summarized in § 6. A value for the Hubble constant of

$H_0 = 70 \text{ km s}^{-1} \text{ Mpc}^{-1}$  is assumed throughout this work.

## 2. DATA SAMPLE AND TEMPLATE RC DERIVATION

A compilation of *I*-band photometry and rotational width data (obtained from long-slit optical rotation curves and/or spatially integrated H I-line profiles) for several thousand spiral galaxies has been assembled by our group with the principal purpose of mapping the peculiar velocity field in the local Universe. This sample, referred to as SFI++, includes several already published data sets (CHG05; Springob et al. 2005; Vogt et al. 2004; Dale & Giovanelli 2000, and references therein) along with recently obtained observations; details of this compilation will be fully discussed elsewhere (Masters 2005; Springob 2005). Most notably, SFI++ includes the southern spiral galaxy sample of Mathewson and collaborators (MFB sample; Mathewson, Ford, & Buchhorn 1992; Mathewson & Ford 1996). The *I*-band isophotal photometric fits and RCs derived from long-slit optical spectroscopy for the MFB sample are available to us in digital form, and were reprocessed to achieve consistency with the rest of SFI++ (photometric quantities and rotational widths have been extracted according to the methods described in Haynes et al. 1999 and CHG05, respectively).

In this work, we use the subset of galaxies in the SFI++ sample for which high quality long-slit  $\text{H}\alpha/\text{[N II]}$  RCs and *I*-band photometry are available. Long-slit spectra are of high quality when an extended RC can be reliably extracted, i.e. when the  $\text{H}\alpha$  emission line has high signal-to-noise, is extended, and allows to adequately trace the shape of the RC across its spatial extent. Analogously, *I*-band images are of high quality when photometric parameters can be reliably extracted (i.e., photometric quality, no stars superimposed on the galaxy, object not close to the edge of the frame, etc. Also discarded are cases in which the images are of high quality but the fits are poor because of the presence of a bar, asymmetries, or other problems). Template RCs were obtained by binning the galaxies in *I*-band luminosity intervals, and computing the average RC in each bin as described below. Two separate sets of solutions were derived by adopting different spatial parameterizations, in which the radial coordinates of the RCs are expressed in units of the *I*-band disk scale length,  $r_d$ , or the optical radius,  $R_{\text{opt}}$  (i.e., the radius within which 83% of the total *I*-band light is included, as in PSS96. Notice that  $R_{\text{opt}}$  is a cumulative quantity and not an isophotal radius). The template RCs were then fitted with the analytic function:

$$V_{\text{PE}}(r) = V_0(1 - e^{-r/r_{\text{PE}}})(1 + \alpha r/r_{\text{PE}}) \quad (1)$$

referred to as the *Polyex* model (Giovanelli & Haynes 2002), where  $V_0$ ,  $r_{\text{PE}}$ , and  $\alpha$  respectively determine the amplitude, the exponential scale of the inner region, and the slope of the outer part of the RC (for template RC fitting,  $r$  and  $r_{\text{PE}}$  are expressed in units of  $r_d$  or  $R_{\text{opt}}$ ). Equation 1 is an empirical expression that fits well a large variety of RC shapes (including those declining at large radii), as discussed in CHG05. Alternative fitting functions have been proposed by other authors (e.g., Courteau 1997; Kravtsov et al. 1998; Vogt et al. 2004); since they are all empirical, trade-offs between simplicity and detail result. A comparison between Polyex and

other fitting expressions is beyond the scope of this paper and will not be discussed here.

All the individual RCs used for the derivation of the template curves were fitted using Equation 1 and, although their Polyex parameters were not used in this work, a quality code based on the goodness of the fit was used to select those included in the final sample. For reasons that will be clarified later, the following objects were also not used to construct template RCs: (a) galaxies with inclinations to the line of sight  $i \geq 80^\circ$  (see also §4); (b) galaxies with absolute  $I$ -band magnitude lying outside the  $[-24.0, -18.0]$  interval; (c) RCs with spatial extent smaller than  $2 r_d$  or  $0.6 R_{\text{opt}}$ , for the  $r_d$  and  $R_{\text{opt}}$  parameterizations, respectively; and (d) RCs with average velocity (computed over the spatial interval  $\Delta r$ , as defined in [3] below) incompatible with the value obtained using all the RCs in the same luminosity bin (over the same  $\Delta r$ ). Most of the rejected objects fell into category [a] (472 out of 2777 galaxies in the initial sample). Also, because of the selection criterion [c], the sizes of the final data sets used to derive  $r_d$  and  $R_{\text{opt}}$  template RCs, hereafter referred to as “ $r_d$  and  $R_{\text{opt}}$  samples”, were slightly different, including 2155 and 2169 galaxies respectively.

After binning the galaxies by luminosity, template RCs were obtained as follows:

(1) *Folding* – Each RC was folded about its center of symmetry, as determined by fitting a URC model (PSS96) to the unfolded RC. As pointed out elsewhere (see references in § 1), the URC parameterization is inadequate to model individual RCs, but it approximates the overall RC shape well enough for the purpose of determining its center of symmetry, as argued in CHG05, where our folding technique is described in detail.

(2) *Rescaling and Resampling* – The radial variable of each folded RC was scaled by the  $r_d$  ( $R_{\text{opt}}$ ) value of the galaxy, and the RC amplitude was deprojected to the edge-on view. Inclinations were obtained from ellipticities measured from isophotal fits to the  $I$ -band images, and corrected for seeing effects, following the prescriptions of Giovanelli et al. (1997). RC amplitudes were then resampled on a fixed spatial grid of spacing  $0.1 r_d$  ( $0.03 R_{\text{opt}}$ ) using a linear interpolation including the four observed points nearest to the grid position. This assures that RCs of nearer galaxies, with denser spatial sampling, do not bias the average RCs. We have tested that the results are not sensitive to the choice of the spatial bin centers. Only the resampled RCs were used after this point.

(3) *Normalization* – Obtaining an average RC for each luminosity class requires attention to the fact that the RC of each galaxy is sampled out to a different maximum radius  $R_{\text{max}}$ . To determine the average amplitude of the template RC of a given luminosity class, we thus used only the section  $\Delta r$  between  $2r/r_d$  and  $3r/r_d$  ( $0.6-0.9 r/R_{\text{opt}}$ ) of each RC. Over this interval, nearly all RCs are well sampled (91% of the RCs in the  $r_d$  sample and 95% of those in the  $R_{\text{opt}}$  one extend beyond  $2.5 r/r_d$  and  $0.75 r/R_{\text{opt}}$ , respectively) and exhibit relatively mild gradients. Using a range of radii rather than a single radial position also limits shot noise effects. The normalization of the RCs less extended than  $3 r_d$  ( $0.9 R_{\text{opt}}$ ) was performed using the available points within  $\Delta r$  (29 RCs in

the  $r_d$  sample were normalized using the velocity at  $2.0 r_d$ ). For each RC, we thus measured the average rotational velocity  $v_{\Delta r, i}$ ; objects without a meaningful determination of that parameter have been excluded from our final sample. For a given luminosity class  $M$ , the template RC was obtained by scaling each RC by the ratio  $R_{v,i} \equiv v_{\Delta r, i} / \langle v_{\Delta r, M} \rangle$ , where  $\langle v_{\Delta r, M} \rangle$  is the average  $v_{\Delta r, i}$  for the class (objects with  $R_{v,i} \geq 2$ , corresponding to a  $5\sigma$  deviation from the mean of the distribution for the whole sample, were discarded). The  $1\sigma$  dispersion of the  $v_{\Delta r, i}$  velocities is, on average, 17% of  $\langle v_{\Delta r, M} \rangle$  (it varies between 14% and 22% among the different luminosity classes;  $\langle v_{\Delta r, M} \rangle$  values are listed in Tables 1 and 2, presented in §3). We refer to the RCs scaled in this way as *normalized* RCs.

(4) *Averaging* – Mean velocities and variances were computed (after clipping at the  $2\sigma$ -level) for each grid value of  $r/r_d$  ( $r/R_{\text{opt}}$ ) for which there were at least 4 valid samples, and for each luminosity class. The choice of 4 samples represents a good compromise between maximizing the number of radial bins for the computation of the template RCs and keeping enough points within each radial bin to calculate a meaningful average velocity. Since the scatter of the RCs around the template is artificially reduced over and near the interval  $\Delta r$  where the velocity normalization was performed, we replaced the velocity variance at each grid point (over the entire spatial range covered by the template RC, not just  $\Delta r$ ) with that computed using the unnormalized RCs. In other words, the template RC points were computed using normalized RCs, but the corresponding dispersions are those of the *unnormalized* RCs.

(5) *Smoothing* – The resulting average RCs were Hanning-smoothed, and every other point was recorded, yielding a grid spacing of  $0.2 r_d$  ( $0.06 R_{\text{opt}}$ ). As mentioned above, each template RC point was computed by averaging at least 4 samples (mean velocities resulting from the average of 3 or less points were not recorded). The final template RC points were obtained by expanding underpopulated spatial bins (i.e., bins resulting from the average of  $4 \leq N < 10$  individual RC points) in order to include at least 10 samples. Positions and error bars of the expanded bins are given by the average of the corresponding quantities for the replaced bins.

The binning into luminosity classes was initially done with a constant step  $\Delta M=0.4$ . The bins at the faint end of the interval were expanded, however, to avoid the overlap of the corresponding template RC solutions; in particular, two classes  $M_i$  and  $M_j$  were combined if  $|\langle v_{\Delta r, M_i} \rangle - \langle v_{\Delta r, M_j} \rangle| \leq 10 \text{ km s}^{-1}$ . The final 10 luminosity classes span the  $I$ -band absolute magnitude interval  $[-24.0, -18.0]$  (18 objects with luminosities outside this range were discarded).

The derivation of the template RCs was identical for the  $r_d$  and  $R_{\text{opt}}$  parameterizations, except for the values of the grid spacing and the normalization interval  $\Delta r$  (as in [2] and [3] above). For the  $R_{\text{opt}}$  template RCs, grid spacing and  $\Delta r$  were chosen to match the corresponding  $r_d$  ones, taking into account that the average value of the  $R_{\text{opt}}/r_d$  ratio is  $3.31 \pm 0.01$  for the sample used to construct  $r_d$  template RCs.

As discussed in § 4, the inner slope of observed  $\text{H}\alpha/\text{[N II]}$  RCs depends on inclination, due to internal ex-

tinction in the inner regions of disks. The impact of dust attenuation is more severe for edge-on disks and for intrinsically brighter systems. For this reason, 472 galaxies with inclination  $i \geq 80^\circ$  were excluded from the analysis, as already mentioned. Seeing may also systematically bias the inner slopes of observed RCs, especially for more distant galaxies. The set of galaxies used to construct the template RCs consists of relatively nearby, large spirals, of median recession velocity  $\sim 7000 \text{ km s}^{-1}$  and isophotal radius  $r_{I23.5} \sim 30''$ . We investigated a possible dependence of the shape of RCs on galaxy distance, and found no significant effect for objects in our sample. As another way of testing the impact of seeing on RC shape, we divided our sample into 3 intervals of (linear) disk scale length  $R_d$  ( $R_d < 2 \text{ kpc}$ ,  $2 \text{ kpc} \leq R_d < 3 \text{ kpc}$ , and  $R_d \geq 3 \text{ kpc}$ ) and recomputed the template RCs forcing the same velocity normalization obtained for the whole  $r_d$  sample (as done in § 4 for the inclination classes). We found that galaxies with larger  $R_d$ 's tend to have slightly larger rotational velocities than ones with smaller  $R_d$ 's; however the effect is small (well within the  $1\sigma$  error bars on the template RC velocities. In particular, the maximum velocity difference is of the order of  $20 \text{ km s}^{-1}$  or less for the template RCs in the central luminosity bins,  $-22.8 < M_I < -20.8$ ; there are no galaxies with  $R_d < 2 \text{ kpc}$  in the two brightest bins, nor ones with  $R_d \geq 3 \text{ kpc}$  in the two faintest bins. Larger velocity differences are observed for the  $M_I = -22.8$  case, but the  $R_d < 2 \text{ kpc}$  result is uncertain due to small number statistics) and limited to the  $r < r_d$  spatial interval.

### 3. TEMPLATE RCS: RESULTS AND COMPARISON OF THE TWO PARAMETERIZATIONS

Figure 1 shows the template RCs expressed as functions of exponential disk scale lengths  $r_d$ , obtained by averaging the data in each of 10 luminosity intervals. Each curve is labeled by its mean  $I$ -band absolute magnitude (as listed in column 3 of Table 1, described below); the interval  $\Delta r$  over which the velocities are normalized within each luminosity class is indicated by dotted lines. For each template, the outermost spatial bins have been expanded to include at least 10 elements; hence their spacing from adjacent points is not exactly  $0.2 r/r_d$ . The error bars are Poisson errors on the mean, calculated using unnormalized RCs (see [4] in § 2). Notice that the error bars on the outermost points may not be accurate due to small number statistics. Polyex (see eq. 1) fits to the template RC data points are shown as solid lines. Our results show a smooth transition of RC shapes from small to more massive (luminous) systems, with the latter being characterized by a steeper initial velocity rise and a flatter outer slope. Even in the case of the most luminous bins we see no convincing evidence of velocity decline *within the spatial scales sampled here*, contrarily to what expected based on the URC predictions. In fact, while the very outermost points of the template RCs show a small velocity decrease in a few cases (e.g., those labeled  $-19.37$  and  $-22.60$  in the figure), there is no systematic trend that indicates a falling RC within at least 5 disk scale lengths (6 for the central luminosity bins). In other words, if we were to determine the outer slope of each template RC by fitting a first order polynomial beyond 2 or 3  $r_d$ , none of the fits would have a negative slope. Notice also that the curve labeled  $-21.80$  appears

to decline beyond  $\sim 5 r_d$ , but the two adjacent templates ( $-21.41$  and  $-22.19$ ) have rising outer slopes. This issue will be further discussed in § 5, where we compare our average RCs with those derived by PSS96, upon which the URC parameterization is built. Lastly, we point out that the *bump* at large radii seen for the lowest luminosity template RC is caused by a lack of faint galaxies with extended RCs. In fact, bright galaxies in that luminosity bin (i.e., those with  $M_I < -19.5$ ) span all values of RC extent (up to  $6 r_d$ ), whereas fainter ones ( $M_I > -19$ ) have RCs that extend up to  $4 r_d$  at most (with only one exception, a RC with  $M_I = -18.6$  and  $R_{\max} = 4.8 r_d$ ).

In order to illustrate the actual spread in RC shapes and amplitudes within each luminosity class, we include a version of Figure 1 in which the error bars represent the dispersion around the mean (Figure 2). Typical values of the standard deviation around the mean are  $13 \text{ km s}^{-1}$  for the template RCs in the lowest 4 luminosity bins,  $30 \text{ km s}^{-1}$  for the one labeled  $-23.76$ , and  $20 \text{ km s}^{-1}$  for the others.

Table 1 summarizes the statistics for each luminosity class and provides the values of the Polyex parameters of the template RC fits shown in Figures 1 and 2. The quantities listed are:

*Column (1):* center of the luminosity bin,  $M_I$ , in magnitude units.

*Column (2):* width of the luminosity bin,  $\Delta M_I$ .

*Column (3):* mean value of the absolute  $I$ -band magnitude within the corresponding bin,  $\langle M_I \rangle$ .

*Column (4):* mean velocity of the RCs,  $\langle v_{\Delta r, M} \rangle$ , measured between  $2r_d$  and  $3r_d$ . This value is used to normalize the velocities of the individual RCs belonging to the same luminosity bin, as explained in § 2 (item [3]).

*Column (5):* number of RCs included in each luminosity bin,  $N_{\Delta r, M}$ .

*Columns (6)–(8):* coefficients of the Polyex model (see eq. 1) fits to the template RCs, with errors;  $V_0$  is measured in  $\text{km s}^{-1}$ ,  $r_{\text{PE}}$  is expressed in units of  $r_d$ , and  $\alpha$  is dimensionless.

The bin centered at  $M_I = -23.8$  contains only 43 objects, but is particularly interesting because the most luminous galaxies are expected to show the most declining RCs within a few disk scale lengths (based on URC predictions), implying a rather small contribution of the dark matter component to the internal kinematics of such systems. The fastest rotators represent also important tools to test our understanding of galaxy formation and disk stability (e.g., Spekkens 2005; see also § 5).

The variations of the Polyex parameters with  $I$ -band absolute magnitude are displayed in Figure 3. The trend seen in the top panel reflects the well-known result that brighter disk galaxies rotate faster (the TF relation); the other two panels show that RCs of brighter systems have steeper velocity increase within the inner regions and flatter outer slopes.

The results for the template RCs expressed as functions of optical radii rather than disk scale lengths are presented in Figures 4, 5, 6, and Table 2 (analogous to Figures 1, 2, 3, and Table 1 respectively). As mentioned in § 2, the interval  $\Delta r = 0.6\text{--}0.9 r/R_{\text{opt}}$  for velocity normalization within each luminosity class corresponds to  $\Delta r = 2\text{--}3 r/r_d$  for an average  $R_{\text{opt}}/r_d$  ratio of 3.3, as determined for the 2155 galaxies of the  $r_d$  sample. The difference between the corresponding values of the velocity

normalization (listed in column 4 of Tables 1 and 2), is smaller than  $3 \text{ km s}^{-1}$  for all the luminosity bins except the  $M_I = -23.8$  one, where the discrepancy is slightly larger ( $5.4 \text{ km s}^{-1}$ ). A quick inspection of the two tables also reveals that the numbers of RCs belonging to the same luminosity bin are similar, but not the same, for the  $r_d$  and  $R_{\text{opt}}$  samples. Such small differences are caused by the exclusion of RCs that are spatially less extended than  $2 r_d$  or  $0.6 R_{\text{opt}}$  and by the fact that the  $R_{\text{opt}}/r_d$  distribution is not a delta function centered on 3.3. In fact, if we dropped the restriction on RC extent, or if all the RCs had  $R_{\text{opt}}=3.3 r_d$ , the composition of the two samples used for template RC derivation and their distribution into luminosity classes would be identical. In practice, for instance, a RC with a maximum extent  $R_{\text{max}}=2.1 r_d$  is part of the  $r_d$  sample, but will be included in the  $R_{\text{opt}}$  sample only if  $R_{\text{opt}}/r_d \leq 3.5$ ; viceversa, a RC with  $R_{\text{max}}=1.9 r_d$  will be missing from the  $r_d$  set and included in the  $R_{\text{opt}}$  one if  $R_{\text{opt}}/r_d \leq 3.2$ . A comparison between the distributions of  $R_{\text{opt}}/r_d$  for the two sets of galaxies (not shown) confirms that the  $R_{\text{opt}}$  sample has a slightly larger (smaller) fraction of objects with  $R_{\text{opt}}/r_d < 3.3$  ( $> 3.3$ ) with respect to the  $r_d$  sample.

When scaled with  $R_{\text{opt}}$  rather than  $r_d$ , the template RCs have flatter outer slopes. As for the  $r_d$  solutions, there are a few examples of templates whose outermost points show a small velocity decrease (Figure 4); however, there is no clear indication of declining RCs within the spatial interval sampled by our data, in the sense that linear fits to the outer regions of the template RCs (beyond 0.6 or  $0.9 R_{\text{opt}}$ ) would have flat or positive slopes. The only exception is the curve labeled  $-22.60$ , but again we notice that the adjacent templates have rising or flat slopes. The solutions obtained with the two parameterizations are very similar, except for the tendency of the  $r_d$  template RCs to show steeper outer slopes, as indicated by the larger values of the Polyex parameter  $\alpha$  in the bottom panel of Figure 3 and in column (8) of Table 1, compared with the corresponding results for the  $R_{\text{opt}}$  case. This effect is clearly illustrated in Figure 7, where the two sets of Polyex fits displayed in Figures 1 and 4 are reproduced as dashed and solid lines, respectively. Excluding the  $M_I = -23.8$  bin, which is also characterized by the poorest statistics, the template RCs obtained with the two parameterizations are nearly indistinguishable within  $r \sim 1 R_{\text{opt}}$ , whereas the  $r_d$  tracings are systematically steeper than the  $R_{\text{opt}}$  ones beyond that radius. If all the RCs had the same  $R_{\text{opt}}/r_d$  ratio, the results would be identical, and in fact the  $r_d$  templates could be obtained directly from the  $R_{\text{opt}}$  ones (or viceversa) by rescaling the horizontal axis. On the other hand, a distribution of  $R_{\text{opt}}/r_d$  values should introduce only scatter, and not a systematic change of RC slopes. In order to explain the observed bias,  $R_{\text{opt}}/r_d$  must be dependent on RC extent, in the sense that RCs sampled out to larger fractions of the disks must also be characterized, on average, by larger  $R_{\text{opt}}/r_d$ . Figure 8 shows the correlation between  $R_{\text{opt}}/r_d$  and RC extent,  $R_{\text{max}}$ , measured in units of disk scale lengths, for the 2155 galaxies of the  $r_d$  data set; the dotted line is at  $R_{\text{opt}}/r_d = 3.3$ , the average value for that sample, and the lack of points with  $R_{\text{max}}/r_d < 2$  is due to a selection effect, as mentioned above. Our data show that for a fixed disk scale length, galaxies with more extended RCs

have, on average, larger optical radii, thus explaining the systematic difference of slopes between the  $r_d$  and  $R_{\text{opt}}$  template RCs seen in Figure 7. We investigated the origin of the correlation between  $R_{\text{opt}}/r_d$  and RC extent by binning the sample into four intervals with different disk central surface brightness  $\mu_0$  (measured from our  $I$ -band profiles and corrected for Galactic and internal extinction, cosmological k-term, and converted to face-on perspective), as indicated in Figure 9, and by coding the objects based on their morphological types (adopting the scheme in the RC3 catalog; de Vaucouleurs et al. 1991). Since our sample is mostly composed of Sb or S... (42%), Sbc (14%), and Sc (36%) galaxies, we grouped the data points into two classes only, Sb and earlier types (asterisks) and Sbc and later types (open squares). Our results indicate that: (a) not surprisingly, the  $\text{H}\alpha$  emission is typically traced to a larger extent in the disks of galaxies with higher surface brightness; (b) the average value of  $R_{\text{opt}}/r_d$  increases with decreasing  $\mu_0$ , as the distribution of data points with respect to the  $R_{\text{opt}}/r_d = 3.3$  line in each panel illustrates; (c) in the upper panel, where the data span the largest  $R_{\text{max}}/r_d$  range, the  $R_{\text{opt}}/r_d$  ratio shows a clear dependence on RC extent; such trend is also present in the central panels, although less convincingly; (d) there is no obvious dependence on morphological type, presence of an identifiable bar (not shown), or  $I$ -band luminosity (not shown). In conclusion, the systematic difference of slopes beyond  $r \sim R_{\text{opt}}$  between the two sets of template RCs in Figure 7 is largely caused by the high surface brightness part of our sample. In the region between 4 and  $6.5 R_{\text{max}}/r_d$ , where the discrepancy is larger, the contribution to the template RC points is dominated by the objects in the two upper panels of Figure 9, which are characterized by an  $R_{\text{opt}}/r_d$  ratio that is systematically larger than the average of the sample, especially for increasing values of  $R_{\text{max}}/r_d$ .

In this section, we have presented template RCs expressed separately as functions of exponential disk scale lengths or optical radii. While the description in terms of  $r_d$  is preferred for its more immediate interpretation in the context of galaxy structure and disk modeling, the  $R_{\text{opt}}$  parameterization is also provided in order to allow a direct comparison between PSS96's and our results (see § 5). From an observational point of view, individual values of  $r_d$  carry significant errors because of the difficulty of fitting exponential slopes in the presence of both spiral structure and radially-dependent extinction. Being a cumulative parameter,  $R_{\text{opt}}$  is more straightforward to measure and is less subject to extinction effects. The complicating presence of a bulge would bias both measurements, in the sense that the estimated values would be systematically smaller than those determined for a galaxy with the same disk but no bulge. The impact on  $R_{\text{opt}}$  would be direct and much larger, possibly introducing morphological and/or luminosity effects.

#### 4. IMPACT OF INTERNAL EXTINCTION ON TEMPLATE RCS

As mentioned in § 2, galaxies with inclination  $i \geq 80^\circ$  were excluded from the sample used to derive the template RCs, in order to minimize the effects of the internal extinction on our results. Here we address this issue in more detail, and motivate our choice of the inclination threshold for inclusion in the final sample.

Several works have previously presented evidence for internal extinction in the inner regions of disk galaxies, based on the analysis of optical and near-infrared photometry or spectroscopy. Extinction affects an observed RC by causing its slope to appear shallower; this effect, first noted by Goad & Roberts (1981), is illustrated by the radiative transfer simulations of Bosma et al. (1992) and Baes et al. (2003). These studies show that dust attenuation has a severe impact on the observed kinematics of edge-on disks, even for modest optical depths, and that such effects are strongly reduced for galaxies that are more than a few degrees from edge-on, becoming entirely negligible for intermediate inclinations. These results were confirmed by the analysis of Giovanelli & Haynes (2002, hereafter GH02), which also showed that the prominence of the effect increases with disk luminosity. Exploiting a substantial fraction of the SFI++ sample used in this work, GH02 showed that the kinematic scale length  $r_{\text{PE}}$  of the inner slope of a RC (as obtained from the Polyex model in eq. 1) starts increasing noticeably for inclinations  $i \gtrsim 70^\circ$ , the increase being larger for more luminous disks. By contrast, the outer slope  $\alpha$  of the observed RCs shows no dependence on inclination. Adopting a simple model for the dust and gas distribution in spiral disks, Valotto & Giovanelli (2004) were able to reproduce the observed trends in GH02 fairly well.

In order to evaluate the impact of internal extinction on our results, we divided our sample, which includes 472 highly inclined ( $i \geq 80^\circ$ ) systems, into 3 inclination intervals and recomputed the template RCs. The results are displayed in Figure 10 for the parameterization in terms of exponential disk scale lengths; only the inner regions are shown. Each panel corresponds to one of the  $I$ -band luminosity classes listed in Table 1, from  $M_I = -23.8$  (a) to  $M_I = -19.0$  (j); different inclination bins are indicated as solid ( $30^\circ \leq i < 70^\circ$ ), dotted ( $70^\circ \leq i < 80^\circ$ ), and dashed ( $80^\circ \leq i \leq 90^\circ$ ) lines. The velocity normalization of the individual RCs in each luminosity class was forced to be the same as that used for the whole  $r_d$  sample, as listed in column 4 of Table 1. Figure 10 clearly shows that: (1) the inner slope of the most edge-on systems is systematically shallower, and (2) the effect is more pronounced for more luminous galaxies and almost disappears for intrinsically fainter systems. In the case of highly inclined galaxies, additional geometric effects can cause the inner slopes of observed RCs to appear shallower. Such effects depend on the thickness of the disk (higher values of disk thickness result in shallower RCs), which is a poorly known quantity, and can account for part of the difference between the highest inclination bin and the lower inclination ones in Figure 10. The interplay between optical depth at the disk center and disk thickness is illustrated in Valotto & Giovanelli (2004).

Our results confirm the previous findings of GH02 (as expected, since they provide a different representation of the same effect for essentially the same data set) and of the other studies mentioned above, and show the importance of excluding the highly inclined disks from the derivation of the template RCs. In particular, our chosen threshold  $i = 80^\circ$  allows us to effectively eliminate the RCs that are most affected by dust attenuation (and geometric effects related to the thickness of the disk), without discarding an excessive fraction of the sample.

## 5. COMPARISON WITH PREVIOUS RESULTS

A similar derivation of average RCs of disk galaxies binned in  $I$ -band luminosity intervals was undertaken by PSS96. Their *sample B* included 616 RCs extending out to  $r \geq 0.8 R_{\text{opt}}$  (about 200 of which beyond  $R_{\text{opt}}$ ), obtained by Persic & Salucci (1995) by deprojecting, folding, and smoothing the  $\text{H}\alpha$  data of Mathewson, Ford, & Buchhorn (1992). The RCs in this sample were normalized to the velocity measured at the radius encompassing 65% of the integrated light (approximately corresponding to  $2.2 r_d$  or  $0.7 R_{\text{opt}}$  for a pure exponential disk), separated into 11 luminosity intervals, and averaged in radial bins of size  $0.1 R_{\text{opt}}$ . In order to characterize the velocity field of galactic disks beyond the optical radius, this data set was complemented by *sample A*, a compilation of 131 RCs obtained from published optical or 21 cm  $\text{H}$  I-line spectroscopy. Outer gradients of RCs, defined as the fractional variation  $\delta$  of the rotational velocity between 1 and  $2 R_{\text{opt}}$ , were calculated for 27 RCs in *sample A* extending to about  $2 R_{\text{opt}}$  (mostly  $\text{H}$  I data), and for 5 synthetic RCs obtained from the RCs in *sample B*, “suitably co-added in order to probe the kinematics of the outermost regions.” The variation of  $\delta$  as a function of  $B$ -band absolute magnitude was then used to *extrapolate* the average RCs out to  $2 R_{\text{opt}}$ . The resulting RC tracings were fitted with a parametric form, obtained as the combination in quadrature of an exponential disk and a dark matter halo, and the fit coefficients expressed as functions of luminosity. Based on this parameterization, shapes and amplitudes of *observed* RCs at any radius are completely determined by galaxy luminosity, implying the existence of a universal RC, as originally proposed by Persic & Salucci (1991).

The inadequacy of the URC to model individual RCs has been pointed out by several authors, as mentioned in § 1. Here, we want to compare PSS96’s average RCs in luminosity bins (see their Figure 4) with our template RCs parameterized as functions of optical radii. For this purpose, the Polyex fits shown in Figure 4 are reproduced in Figure 11 as solid lines, overlaid on the URC data points (kindly provided by Paolo Salucci). Since there seems to be a systematic offset between PSS96 and our  $I$ -band luminosity scales (the  $M_I$  bins for the URC tracings are, from top to bottom:  $-23.2, -22.3, -22.0, -21.6, -20.9, -20.5, -20.0, -19.4, -18.5$ ), but the rotational velocity range sampled by our two samples is the same, we optimized the velocity match at the optical radius by shifting all the URC data points by  $+10 \text{ km s}^{-1}$ . As mentioned in § 2, Mathewson, Ford, & Buchhorn (1992) data set is included in our sample, but was reprocessed by us in the same fashion as the rest of SFI++. Therefore the discrepancy between absolute magnitudes might be due to a number of factors, including apparent magnitude measurements, extinction corrections, and distance estimates to the objects (notice that the value of the Hubble constant adopted by PSS96,  $75 \text{ km s}^{-1} \text{ Mpc}^{-1}$ , is very similar to the one used in this work). The comparison between PSS96 and our average RCs should be carried out separately for the two spatial intervals below and above  $R_{\text{opt}}$ , due to the different nature of the corresponding URC points, as summarized at the beginning of this section. Below  $R_{\text{opt}}$ , where the URC points were obtained

by averaging RC data, the agreement is fairly good, especially for the 5 lower luminosity bins (in the case of the curves labeled  $-22.2$  and  $-22.6$ , one should interpolate between the two nearest template RCs in order to obtain one that matches the URC velocity at  $R_{\text{opt}}$ ). There is however a systematic tendency for the URC tracings to have shallower slopes, in particular for the higher luminosity bins (although their noise is larger), an effect that might be caused by the inclusion of edge-on systems in PSS96 analysis (see § 4). Beyond  $R_{\text{opt}}$ , where the URC points were derived from linear extrapolations mostly based on H I data, the agreement is good for the 3 lower  $M_I$  bins and becomes increasingly worse at higher luminosities. In particular, the URC extrapolations for the curves labeled  $M_I < -22$ , characterized by slopes that vary from marginally to strongly *declining*, are inconsistent with our Polyex fits. Interestingly, the results obtained by PSS96 by co-adding the RCs of their *sample B* in 5 luminosity bins show no indications of a velocity decrease within  $2 R_{\text{opt}}$ . In particular, the curve labeled  $M_I = -22.6$  in their Figure B2 (which would lie between the two uppermost URC tracings in Figure 11) has an outer gradient  $\delta \simeq 0$ , indicating a flat RC slope between 1 and  $2 R_{\text{opt}}$ . As their Figure 3 shows, the  $\delta$  values for the 5 synthetic RCs are systematically larger than those derived for the individual objects in *sample A*; however, they are also represented with very large error bars and said to be consistent with the others. The URC tracings shown in Figure 11 (with error bars removed for clarity) are compared with the  $R_{\text{opt}}$  template RC data points in Figure 12. The URC solutions qualitatively follow the trend of the template data in the lower luminosity bins, but do not recover the *shapes* of our average RCs at higher luminosities. For instance, the data points of the  $-23.8$  and  $-23.0$  template RCs lie *near* the URC predictions, but the latter clearly do not represent *fits* to the data. In other words, both inner shapes and outer slopes of those template RCs, as derived from best fits to the data points, are not reproduced by the URC tracings. The disagreement is particularly evident for the  $-23.8$  template RC, where a linear fit to its outer region (say, beyond  $0.7 R_{\text{opt}}$ ) is clearly inconsistent with the strongly declining URC slope.

In summary, our template derivation differs from that of PSS96 in several details, such as the exclusion of the most edge-on systems, the resampling of the RCs to the same spatial resolution, and the normalization to a velocity that is both characteristic of the corresponding luminosity class and computed over a range of radii rather than at a single point. But most importantly, the larger size of our data set allows us to probe the velocity fields of the average RCs beyond  $1 R_{\text{opt}}$  without reducing the number of luminosity bins and with no need for extrapolations. For radial galactocentric distances smaller than  $R_{\text{opt}}$ , where both PSS96 and our derivations are based on a homogeneous data set (although differently processed), the results are fairly consistent, when the larger scatter of the URC data and different selection criteria are taken into account. Beyond  $R_{\text{opt}}$ , the URC extrapolations qualitatively agree with our data only at low luminosities, and are inconsistent for  $M_I < -22$ . PSS96 based their extrapolations on a linear fit to the data points in their Figure 3, where the outer gradient  $\delta$  is plotted as a function of the  $B$ -band absolute magnitude. While it

is unclear why the outer gradients of the 5 average RCs built from their *sample B* are larger than those of the other points shown (mostly based on H I data), a fit to those 5 points would yield results in better agreement with our template RCs.

We conclude that late type, high surface brightness spiral galaxies show no clear indication, *on average*, of declining RCs within at least  $4.5 r_d$  ( $6 r_d$  for most of our  $M_I$  bins), even in the case of the most luminous systems in our sample. Of course, this does not contradict claims of declining RCs at larger distances in the disks. Most notably, Casertano & van Gorkom (1991) obtained extended H I synthesis RCs for two highly-inclined, late spiral galaxies: NGC 2683 and NGC 3521. Their  $I$ -band absolute magnitudes, estimated from the  $B$ -band values using a color index  $B-I=1.78$  appropriate for their morphological type (de Jong 1996), and adopting  $H_0 = 70 \text{ km s}^{-1} \text{ Mpc}^{-1}$ , are  $-20.6$  and  $-22.4$ , respectively. Both galaxies exhibit declining RCs at large radii (the H I extends 15 and 12 optical  $r_d$ , respectively), and are included by Casertano & van Gorkom (1991) in the category of “bright compact galaxies” based on their small values of  $r_d$ . The two RCs also show no decrease in rotational velocity within  $6 r_d$  and are thus consistent with our template results. The maximum rotation velocity of NGC 3521, of the order of  $240 \text{ km s}^{-1}$ , is consistent with the corresponding template RC; the fact that NGC 2683, which is  $\sim 2$  magnitudes dimmer, reaches the same maximum velocity is somewhat puzzling but not wholly surprising, given the expected scatter. Extended RCs from H I aperture synthesis observations were also obtained by Spekkens (2005) for eight of the fastest known rotators, with the purpose of investigating the role of disk stability in setting the observed upper limit to the rotational velocities of spiral galaxies. This is a very interesting issue, since it is unclear that the most massive disks can be stabilized by the same processes invoked for less massive systems; in fact, alternative scenarios have been proposed (see Spekkens 2005 and references therein), one of which predicts roughly flat RCs (Sellwood & Moore 1999). For the eight objects in her sample (extracted from SFI++), Spekkens produced hybrid  $\text{H}\alpha + \text{H I}$  RCs with extents ranging from  $1.8$  to  $3.3 R_{\text{opt}}$ . All these RCs are remarkably flat beyond  $R_{\text{opt}}$  (about half showing a very mild velocity decline for  $r > 1.5 - 2 R_{\text{opt}}$ ) and in qualitative agreement with our template solutions.

## 6. DISCUSSION AND CONCLUSIONS

Taking advantage of a large sample of long-slit optical RCs with available  $I$ -band photometry, we have reinvestigated the dependence of RC shape on galaxy luminosity. We determined *template* relations by fitting a function, the Polyex model (eq. 1), to the average RCs calculated in 10 luminosity classes, spanning the  $I$ -band absolute magnitude range  $[-24.0, -18.0]$ . After ascertaining the effect of internal extinction on our results, we excluded the 472 most edge-on systems ( $i \geq 80^\circ$ ) from the analysis. The template RCs are expressed as functions both of exponential disk scale lengths  $r_d$  and of optical radii  $R_{\text{opt}}$ , the latter to allow a direct comparison with PSS96’s average RCs and URC predictions. When scaled with  $r_d$ , the template relations show a smooth transition of RC shapes with increasing  $I$ -band luminosity, with the most luminous systems being char-

acterized by steeper inner velocity rises and flatter outer slopes. The  $R_{\text{opt}}$  templates show analogous variations of RC amplitudes and inner slopes with  $I$ -band luminosity, but their outer slopes are nearly constant. A direct comparison of the two sets of templates shows that the results are very similar within  $R_{\text{opt}}$ ; beyond that radius the  $r_{\text{d}}$  templates have steeper slopes. This difference is mostly attributed to the high brightness galaxies, whose RCs are typically traced further out in the disks, and which are characterized by  $R_{\text{opt}}/r_{\text{d}}$  ratios larger than the average for the rest of the sample. We do not find convincing evidence for declining RCs *within the spatial scales sampled by our data*, i.e. 4.5–6  $r_{\text{d}}$ , even for the most massive systems, in contradiction with the URC models (which, beyond  $R_{\text{opt}}$ , are based on linear extrapolations). As argued in §3, there are a few examples of template RCs whose outermost points show a small velocity decrease, but there is no clear indication of declining outer slopes (as they would be measured from linear fits to the outer regions of the average RCs beyond 2 or 3  $r_{\text{d}}$ , or, equivalently, 0.6 or 0.9  $R_{\text{opt}}$ ). One template RC (the one labeled –22.60 in Figure 4) does appear to be declining beyond  $\sim 1.1 R_{\text{opt}}$ , but the adjacent curves have rising or flat outer slopes. For less luminous objects or below  $R_{\text{opt}}$ , our templates are qualitatively consistent with the URC tracings, when the larger scatter of PSS96’s average RCs and different selection criteria (namely, the exclusion of edge-on galaxies from our analysis) are taken into account. Being significantly larger than the sample upon which the URC is based, our data set allows us to compute average RCs that extend beyond  $R_{\text{opt}}$  without reducing the number of luminosity bins or resorting to extrapolations. Our results are consistent with the declining RCs of Casertano & van Gorkom (1991), since the velocity decrease is observed in H I data that span twice the distance sampled by our optical data, and with the hybrid H $\alpha$ + H I RCs of 8 fast rotators studied by Spekkens (2005), which show remarkably flat or mildly declining outer slopes beyond 1.5  $R_{\text{opt}}$ .

Based on our results we cannot make quantitative inferences about the dynamic role of dark matter in galaxies, because optical RCs alone cannot constrain the properties of dark matter halos on large scales. In fact, a detailed mapping of the radial distribution of visible and dark matter in galaxies requires the use of luminosity profiles and extended H I RCs in addition to optical RCs. Nonetheless, the comparison between Figure 4 and the

URC models suggests that dark matter plays a more significant role in determining the internal kinematics *within the optical disk* of the most luminous systems than what claimed by PSS96. At high luminosity, the profiles of PSS96’s RCs show a strong velocity decrease between 1 and 2  $R_{\text{opt}}$ ; their decomposition into a disk and a dark halo component in terms of the URC parameterization implies a modest dark matter content, whereas low luminosity systems are dark matter dominated. Since the templates RCs of the high luminosity systems do not appear to decline over those spatial scales, their dark matter content within the optical disk based on the URC predictions might be underestimated.

The template RCs, expressed by the Polyex parameters as a function of galaxy luminosity, can be used to constrain models of the circular velocity field of disks, with applications that range from studies of dark matter content and kinematic properties of galaxies, to numerical simulations of disk formation and evolution within the current cosmological framework, and in general studies that, for different reasons, must rely on RC models. Our parameterization in terms of disk scale lengths should prove especially useful in the theoretical and numerical modeling of disk structure and evolution.

The results presented here will be used to determine statistical corrections for aperture bias of emission line widths obtained with fiber spectroscopy, such as those that the on-going Sloan Digital Sky Survey (Strauss et al. 2002) is collecting for one million galaxies. Full rotational velocities of quiescent disk galaxies with apparent sizes larger than the fiber diameter can be statistically recovered by simulating the impact of the finite aperture on the observations, where the galaxy RCs are modeled using our template relations (B. Catinella et al., in preparation; Catinella 2005).

We thank Paolo Salucci for contributing the data points in Figure 11 and K. L. Masters, K. Spekkens and C. M. Springob for communicating results in advance of publication. We also thank our anonymous referee for helpful comments that improved the presentation of this paper. This research was partly supported by a NAIC pre-doctoral research grant at the Arecibo Observatory to BC and by NSF grants AST-9900695 and AST-0307396.

## REFERENCES

Abadi, M. G., Navarro, J. F., Steinmetz, M., & Eke, V. R. 2003, ApJ, 591, 499

Avila-Reese, V., Firmani, C., & Hernández, X. 1998, ApJ, 505, 37

Baes, M., et al. 2003, MNRAS, 343, 1081

Böhm, A., et al. 2004, A&A, 420, 97

Bosma, A., Byun, Y., Freeman, K. C., & Athanassoula, E. 1992, ApJ, 400, L21

Bullock, J. S., Dekel, A., Kolatt, T. S., Kravtsov, A. V., Klypin, A. A., Porciani, C., & Primack, J. R. 2001a, ApJ, 555, 240

Bullock, J. S., Kolatt, T. S., Sigad, Y., Somerville, R. S., Kravtsov, A. V., Klypin, A. A., Primack, J. R., & Dekel, A. 2001b, MNRAS, 321, 559

Casertano, S., & van Gorkom, J. H. 1991, AJ, 101, 1231

Catinella, B. 2005, Ph.D. thesis, Cornell Univ.

Catinella, B., Haynes, M. P., & Giovanelli, R., 2005, AJ, in press (CHG05)

Courteau, S. 1997, AJ, 114, 2402

Dalcanton, J. J., Spergel, D. N., & Summers, F. J. 1997, ApJ, 482, 659

Dale, D. A., & Giovanelli, R. 2000, in ASP Conf. Ser. 201, Cosmic Flows 1999, ed. S. Courteau, M. Strauss, & J. Willick (San Francisco: ASP), 25

de Jong, R. S. 1996, A&A, 313, 377

de Vaucouleurs, G., de Vaucouleurs, A., Corwin, H. G., Buta, R. J., Paturel, G., & Fouqué, P. 1991, Third Reference Catalogue of Bright Galaxies (New York: Springer) (RC3)

Dutton, A. A., Courteau, S., de Jong, R., & Carignan, C. 2005, ApJ, 619, 218

Firmani, C., & Avila-Reese, V. 2000, MNRAS, 315, 457

Garrido, O., Marcelin, M., & Amram, P. 2004, MNRAS, 349, 225

Giovanelli, R., Haynes, M. P., Herter, T., Wegner, G., Salzer, J. J., da Costa, L. N., & Freudling, W. 1997, AJ, 113, 22

Giovanelli, R., & Haynes, M. P. 2002, ApJ, 571, L107 (GH02)

Goad, J. W., & Roberts, M. S. 1981, ApJ, 250, 79

TABLE 1  
RC DISTRIBUTION IN LUMINOSITY CLASSES AND POLYEX MODEL FITS TO  
TEMPLATE RCs PARAMETERIZED AS FUNCTIONS OF EXPONENTIAL DISK SCALE  
LENGTHS

$M_I$ (1)	$\Delta M_I$ (2)	$\langle M_I \rangle$ (3)	$\langle v_{\Delta r, M} \rangle$ (4)	$N_{\Delta r, M}$ (5)	$V_0$ (6)	$r_{\text{PE}}/r_d$ (7)	$\alpha$ (8)
-23.80	0.40	-23.76	285.1	43	$270 \pm 5$	$0.37 \pm 0.02$	$0.007 \pm 0.003$
-23.40	0.40	-23.37	258.4	124	$248 \pm 2$	$0.40 \pm 0.01$	$0.006 \pm 0.001$
-23.00	0.40	-22.98	225.2	225	$221 \pm 1$	$0.48 \pm 0.01$	$0.005 \pm 0.001$
-22.60	0.40	-22.60	198.4	324	$188 \pm 1$	$0.48 \pm 0.01$	$0.012 \pm 0.001$
-22.20	0.40	-22.19	175.7	341	$161 \pm 1$	$0.52 \pm 0.01$	$0.021 \pm 0.001$
-21.80	0.40	-21.80	155.1	327	$143 \pm 1$	$0.64 \pm 0.01$	$0.028 \pm 0.002$
-21.40	0.40	-21.41	137.4	263	$131 \pm 1$	$0.73 \pm 0.02$	$0.028 \pm 0.003$
-21.00	0.40	-21.02	120.7	213	$116 \pm 2$	$0.81 \pm 0.02$	$0.033 \pm 0.005$
-20.40	0.80	-20.48	103.7	203	$97 \pm 2$	$0.80 \pm 0.02$	$0.042 \pm 0.005$
-19.00	2.00	-19.37	79.5	92	$64 \pm 3$	$0.72 \pm 0.05$	$0.087 \pm 0.016$

TABLE 2  
RC DISTRIBUTION IN LUMINOSITY CLASSES AND POLYEX MODEL FITS TO TEMPLATE  
RCs PARAMETERIZED AS FUNCTIONS OF OPTICAL RADII

$M_I$ (1)	$\Delta M_I$ (2)	$\langle M_I \rangle$ (3)	$\langle v_{\Delta r, M} \rangle$ (4)	$N_{\Delta r, M}$ (5)	$V_0$ (6)	$r_{\text{PE}}/R_{\text{opt}}$ (7)	$\alpha$ (8)
-23.80	0.40	-23.76	290.5	44	$275 \pm 6$	$0.126 \pm 0.007$	$0.008 \pm 0.003$
-23.40	0.40	-23.37	260.6	130	$255 \pm 2$	$0.132 \pm 0.003$	$0.002 \pm 0.001$
-23.00	0.40	-22.98	227.8	226	$225 \pm 1$	$0.149 \pm 0.003$	$0.003 \pm 0.001$
-22.60	0.40	-22.60	200.2	328	$200 \pm 1$	$0.164 \pm 0.002$	$0.002 \pm 0.001$
-22.20	0.40	-22.19	176.3	346	$170 \pm 1$	$0.178 \pm 0.003$	$0.011 \pm 0.001$
-21.80	0.40	-21.80	156.5	330	$148 \pm 2$	$0.201 \pm 0.004$	$0.022 \pm 0.002$
-21.40	0.40	-21.41	138.4	267	$141 \pm 2$	$0.244 \pm 0.005$	$0.010 \pm 0.003$
-21.00	0.40	-21.02	121.4	210	$122 \pm 2$	$0.261 \pm 0.008$	$0.020 \pm 0.005$
-20.40	0.80	-20.48	105.1	195	$103 \pm 2$	$0.260 \pm 0.008$	$0.029 \pm 0.005$
-19.00	2.00	-19.38	80.7	93	$85 \pm 5$	$0.301 \pm 0.022$	$0.019 \pm 0.015$

Governato, F., Mayer, L., Wadsley, J., Gardner, J. P., Willman, B., Hayashi, E., Quinn, T., Stadel, J., & Lake, G. 2004, ApJ, 607, 688

Haynes, M. P., Giovanelli, R., Salzer, J. J., Wegner, G., Freudling, W., da Costa, L. N., Herter, T., & Vogt, N. P. 1999, AJ, 117, 1668

Jimenez, R., Verde, L., & Oh, S. P. 2003, MNRAS, 339, 243

Kravtsov, A. V., Klypin, A. A., Bullock, J. S., & Primack, J. R. 1998, ApJ, 502, 48

Mao, S., Mo, H. J., & White, S. D. M. 1998, MNRAS, 297, L71

Masters, K. L. 2005, Ph.D. thesis, Cornell University

Mathewson, D. S., Ford, V. L., & Buchhorn, M. 1992, ApJS, 81, 413

Mathewson, D. S., & Ford, V. L. 1996, ApJS, 107, 97

Mo, H. J., & Mao, S. 2004, MNRAS, 353, 829

Mo, H. J., Mao, S., & White, S. D. M. 1998, MNRAS, 295, 319

Navarro, J. F., Frenk, C. S., & White, S. D. M. 1996, ApJ, 462, 563

Navarro, J. F., Frenk, C. S., & White, S. D. M. 1997, ApJ, 490, 493

Persic, M., & Salucci, P. 1991, ApJ, 368, 60

Persic, M., & Salucci, P. 1995, ApJS, 99, 501

Persic, M., Salucci, P., & Stel, F. 1996, MNRAS, 281, 27 (PSS96)

Roberts, M. S., & Rots, A. H. 1973, A&A, 26, 483

Sellwood, J. A., & Moore, E. M. 1999, ApJ, 510, 125

Simard, L., & Pritchett, C. J. 1999, PASP, 111, 453

Spekkens, K. 2005, Ph.D. thesis, Cornell Univ.

Spekkens, K., Giovanelli, R., & Haynes, M. P. 2005, AJ, 129, 2119

Springob, C. M. 2005, Ph.D. thesis, Cornell University

Springob, C. M., Haynes, M. P., Giovanelli, R., & Kent, B. R. 2005, ApJS, in press

Strauss, M. A., et al. 2002, AJ, 124, 1810

Tully, R. B., & Fisher, J. R. 1977, A&A, 54, 661

Valotto, C., & Giovanelli, R. 2004, AJ, 128, 115

van den Bosch, F. C. 2001, MNRAS, 327, 1334

van den Bosch, F. C. 2002, MNRAS, 332, 456

van den Bosch, F., Abel, T., Croft, R. A. C., Hernquist, L., & White, S. D. M. 2002, ApJ, 576, 21

Verheijen, M. A. W., 1997, PhD thesis, Univ. Groningen

Vogt, N. P., et al. 1997, ApJ, 479, L121

Vogt, N. P., Haynes, M. P., Herter, T., & Giovanelli, R. 2004, AJ, 127, 3273

Willick, J. A. 1999, ApJ, 516, 47

Ziegler, B. L., Böhm, A., Jäger, K., Heidt, J., & Möllenhoff, C. 2003, ApJ, 598, L87

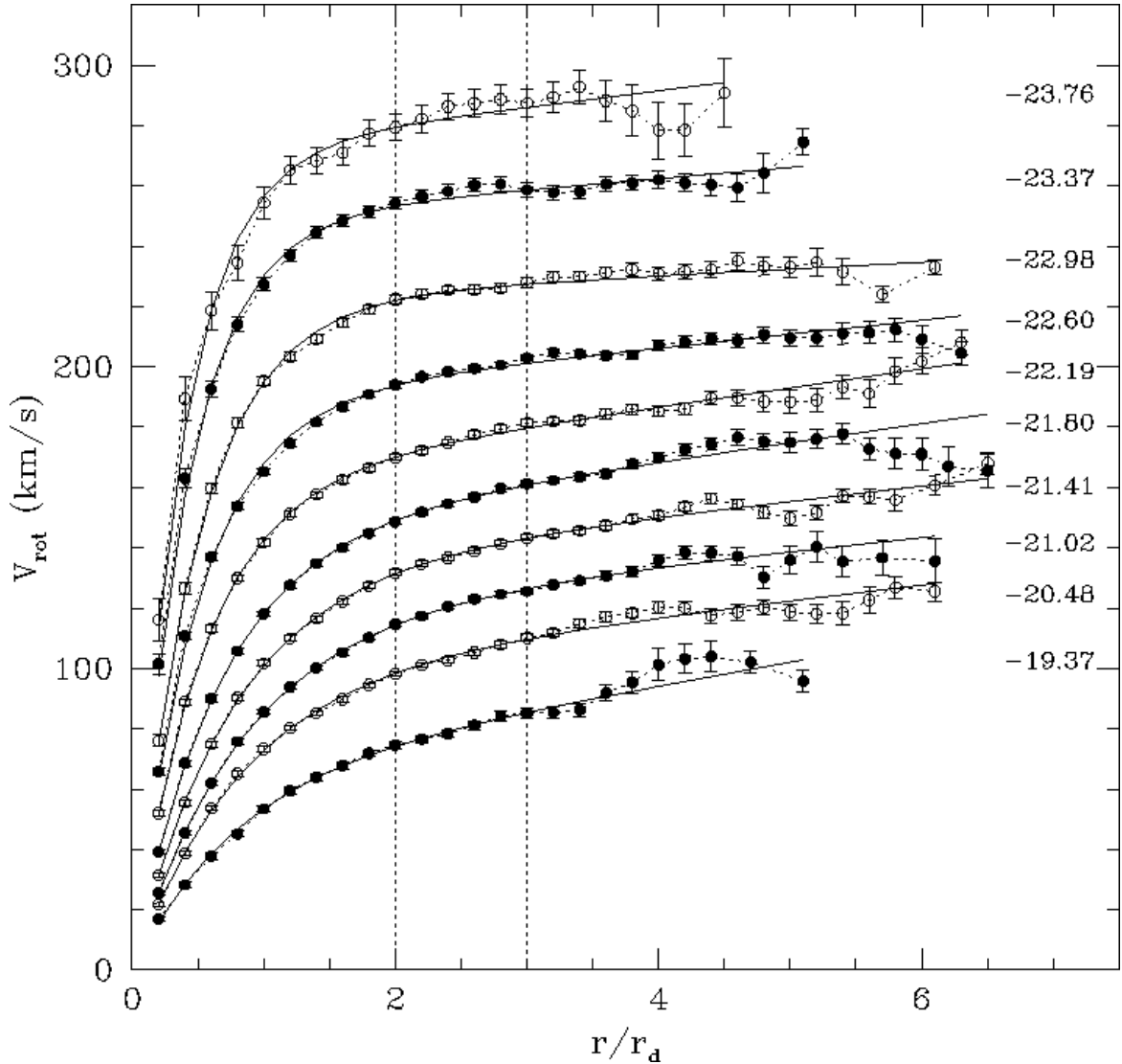


FIG. 1.—Template RCs parameterized as functions of exponential disk scale lengths. Each curve is labeled on the right by its mean  $I$ -band absolute magnitude ( $H_0 = 70 \text{ km s}^{-1} \text{ Mpc}^{-1}$ ). The final sample includes 2155 RCs extending beyond  $2 r_d$ , and with inclination to the line of sight  $i < 80^\circ$ . The vertical, dotted lines show the interval over which the velocity normalization was performed (see §2). The error bars are Poissonian errors on the mean. Polyex fits to the data points are indicated by solid lines; the fit coefficients are presented in Figure 3 and Table 1.

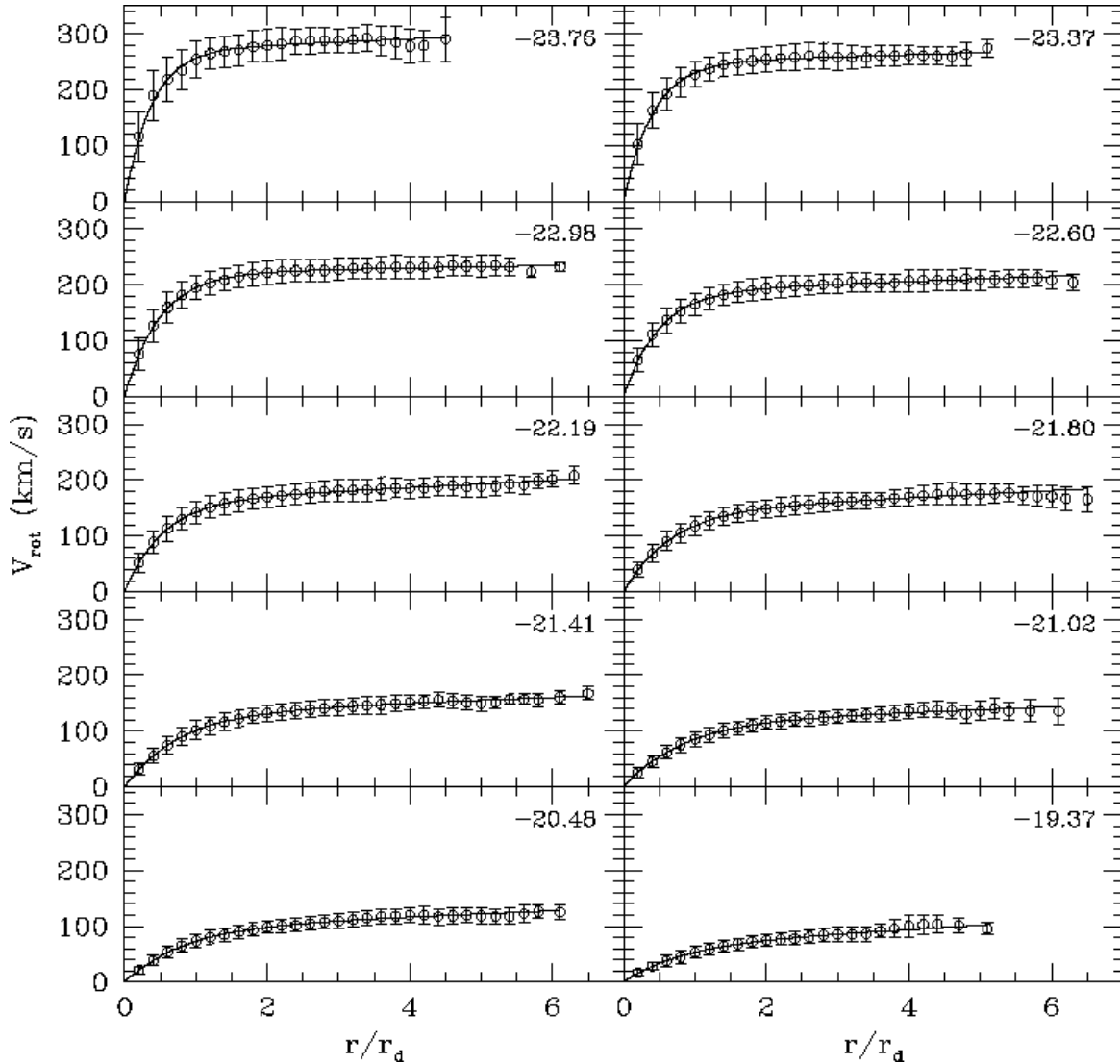


FIG. 2.— The template RCs shown in Figure 1 are displayed here in separate panels, with error bars representing the dispersion around the mean. The solid lines indicate the Polyex fits from Figure 1.

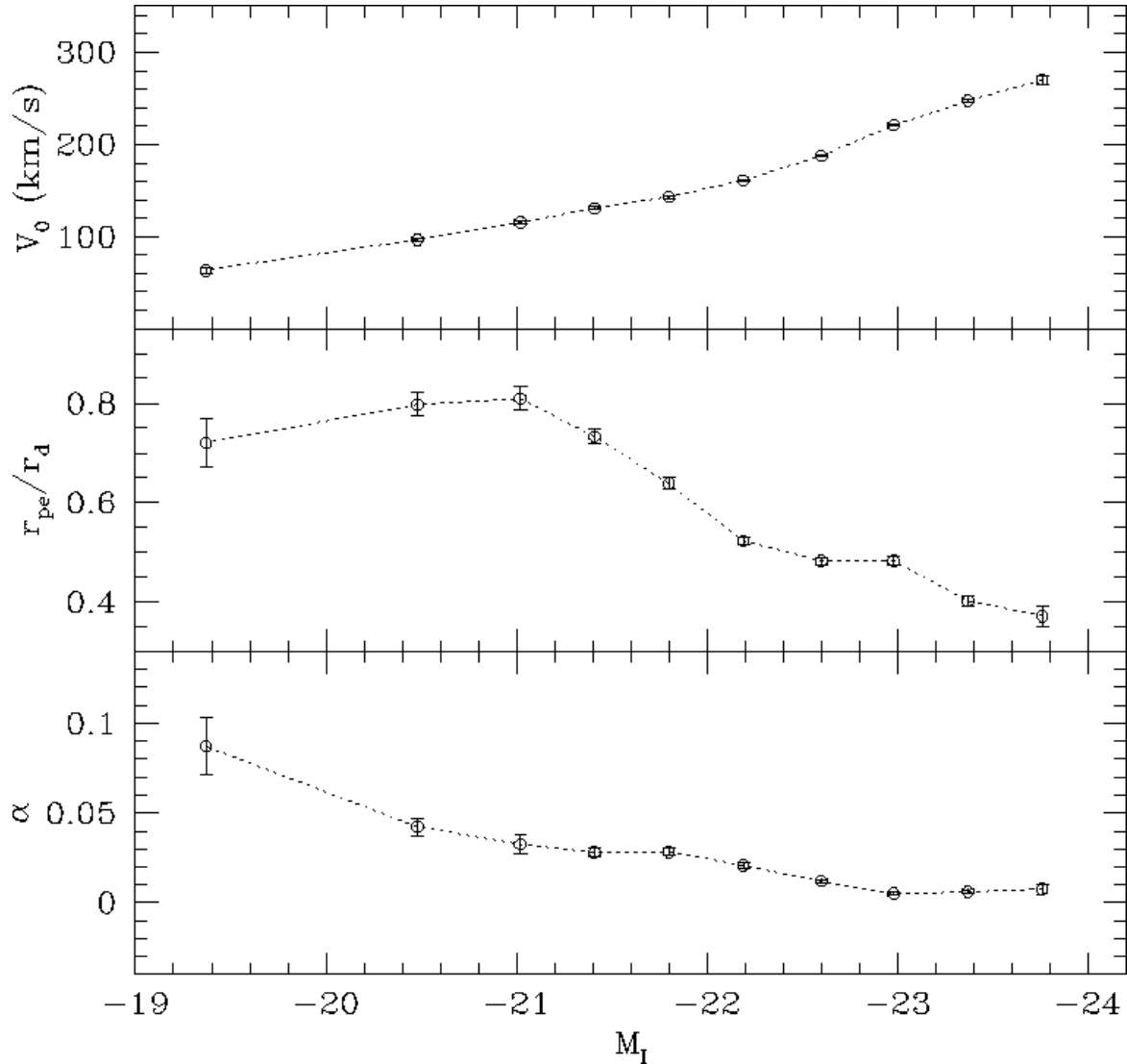


FIG. 3.— Polyex model coefficients of the fits shown in Figure 1, plotted as functions of *I*-band absolute magnitude. See also Table 1.

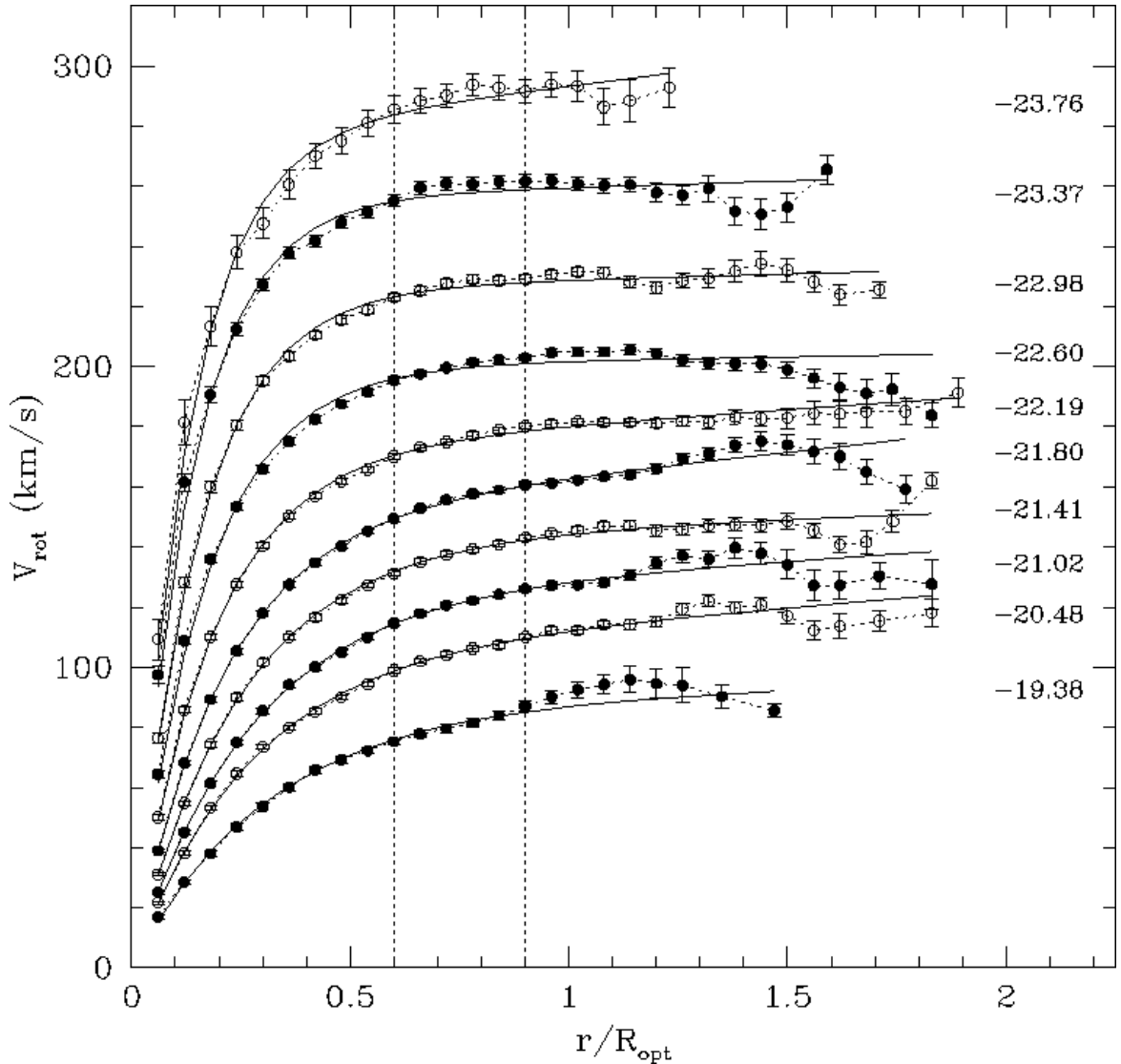


FIG. 4.— Same as Figure 1 for template RCs parameterized as functions of optical radii. This sample includes 2169 RCs extending beyond  $0.6 R_{\text{opt}}$ , and with inclination  $i < 80^\circ$ . Polyex model coefficients are presented in Figure 6 and Table 2.

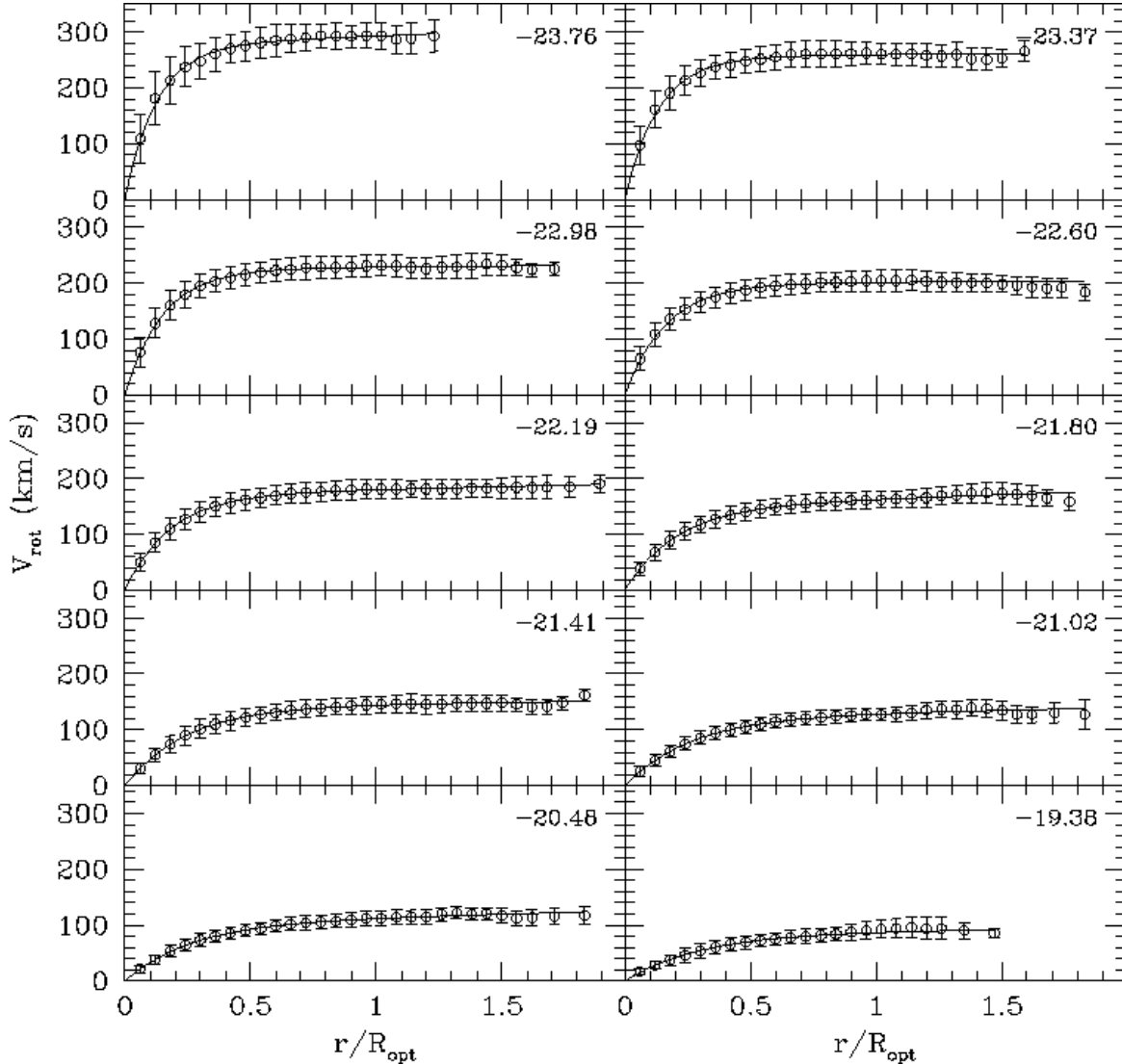


FIG. 5.— Same as Figure 2 for the  $R_{\text{opt}}$  parameterization. The solid lines indicate the Polyex fits from Figure 4.

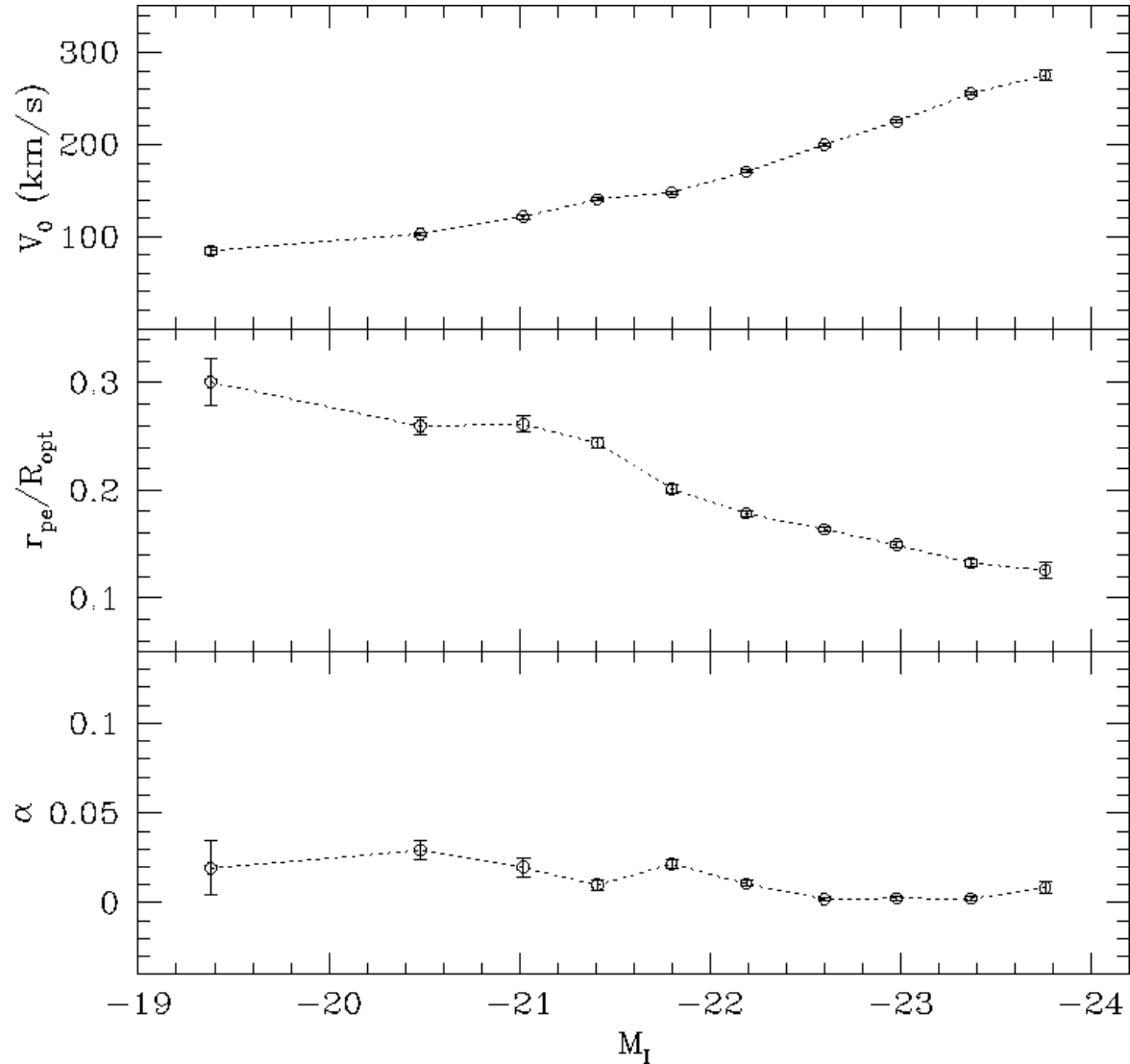


FIG. 6.—Polyex model coefficients of the fits shown in Figure 4; see also Table 2. The vertical scales are the same as those in Figure 3, except for the central panel.

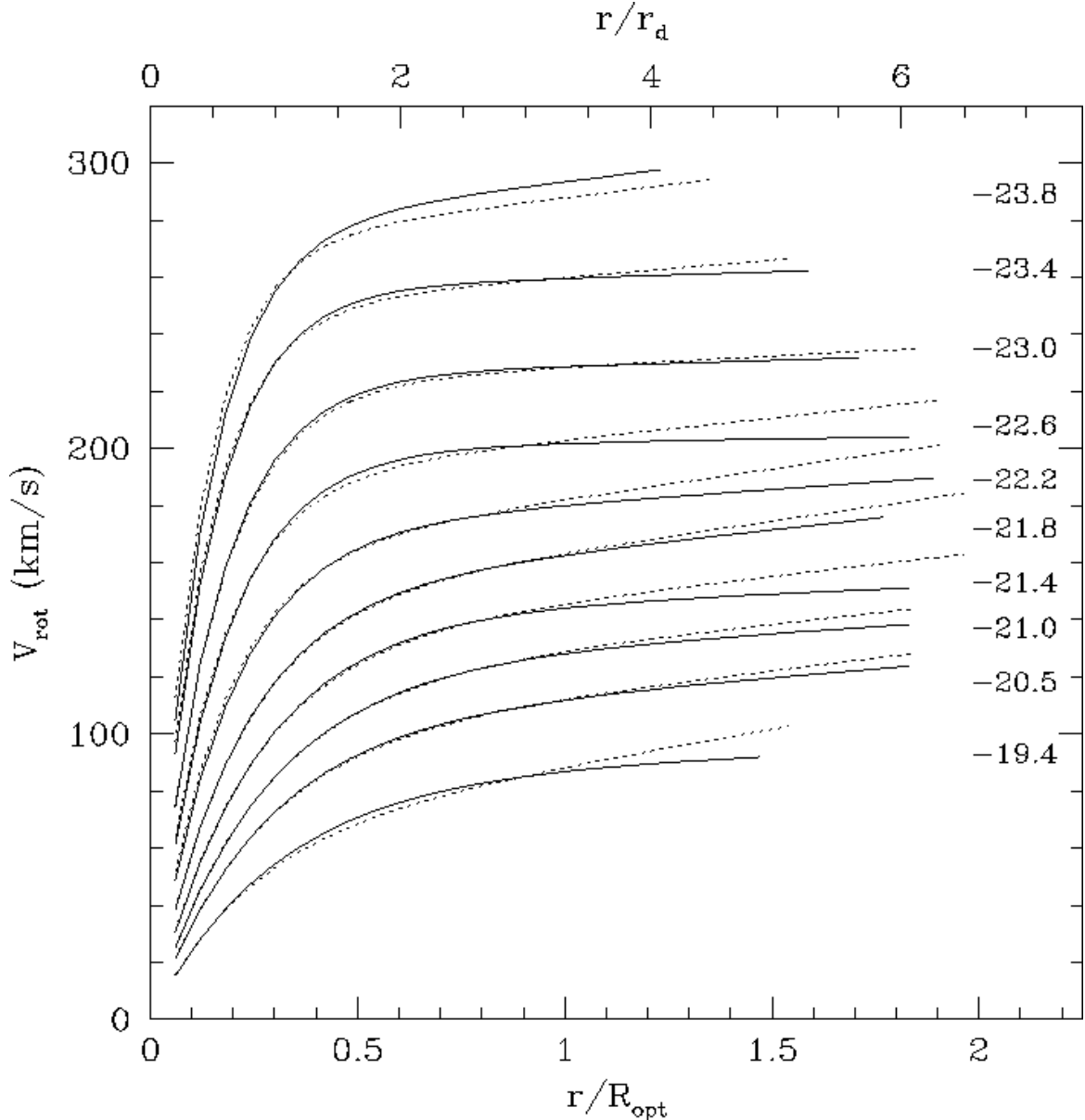


FIG. 7.— Comparison between template RCs expressed in terms of  $R_{\text{opt}}$  (solid lines) or  $r_d$  (dashed). The upper horizontal scale corresponds to the lower one multiplied by a factor 3.3, the average value of the  $R_{\text{opt}}/r_d$  ratio for the galaxies of the  $r_d$  sample.

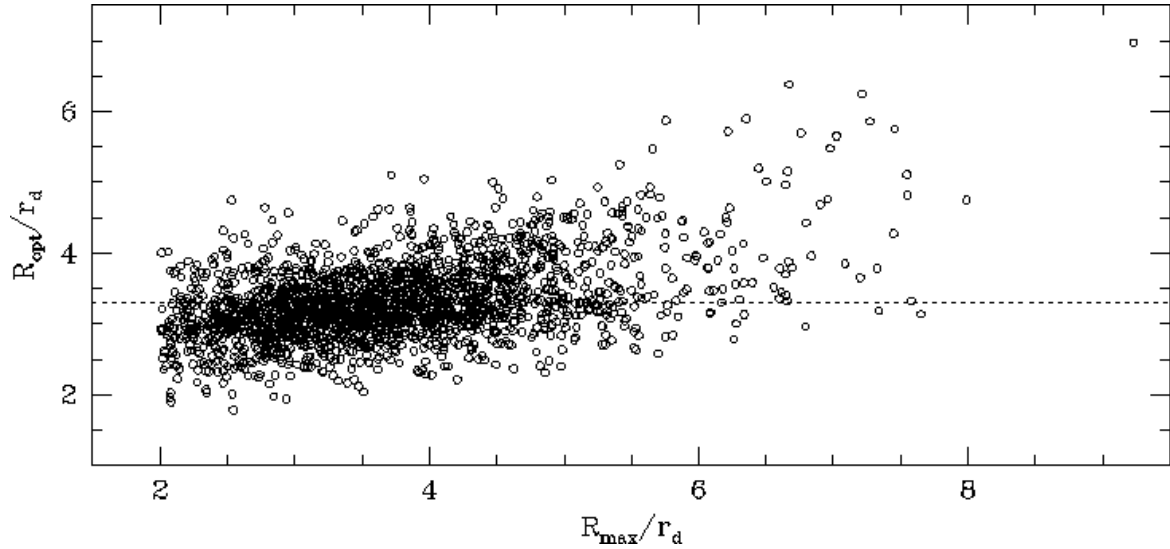


FIG. 8.— Correlation between optical radius and RC extent, both expressed in units of *I*-band exponential disk scale lengths, for the  $r_d$  sample. The dotted line is at  $R_{\text{opt}}/r_d = 3.3$ , the average value for this data set. The trend observed here accounts for the systematic difference of outer slope between the two sets of template RC shown in Figure 7.

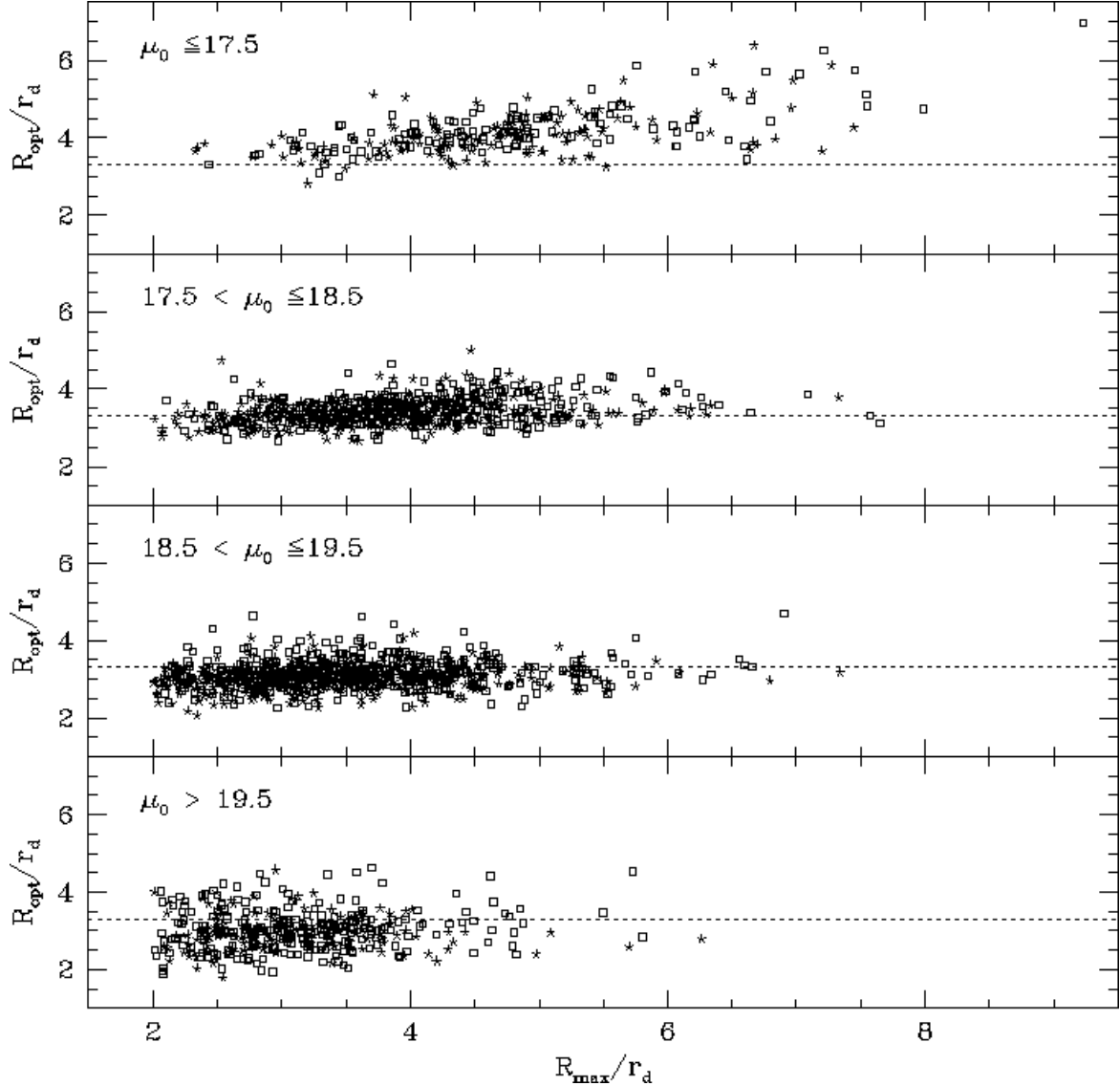


FIG. 9.— Same as Figure 8, with the sample divided into four bins of central surface brightness,  $\mu_0$ , as indicated in each panel. Galaxies with morphological type Sb or earlier are represented by asterisks, those classified as Sbc or later types are marked as open squares.

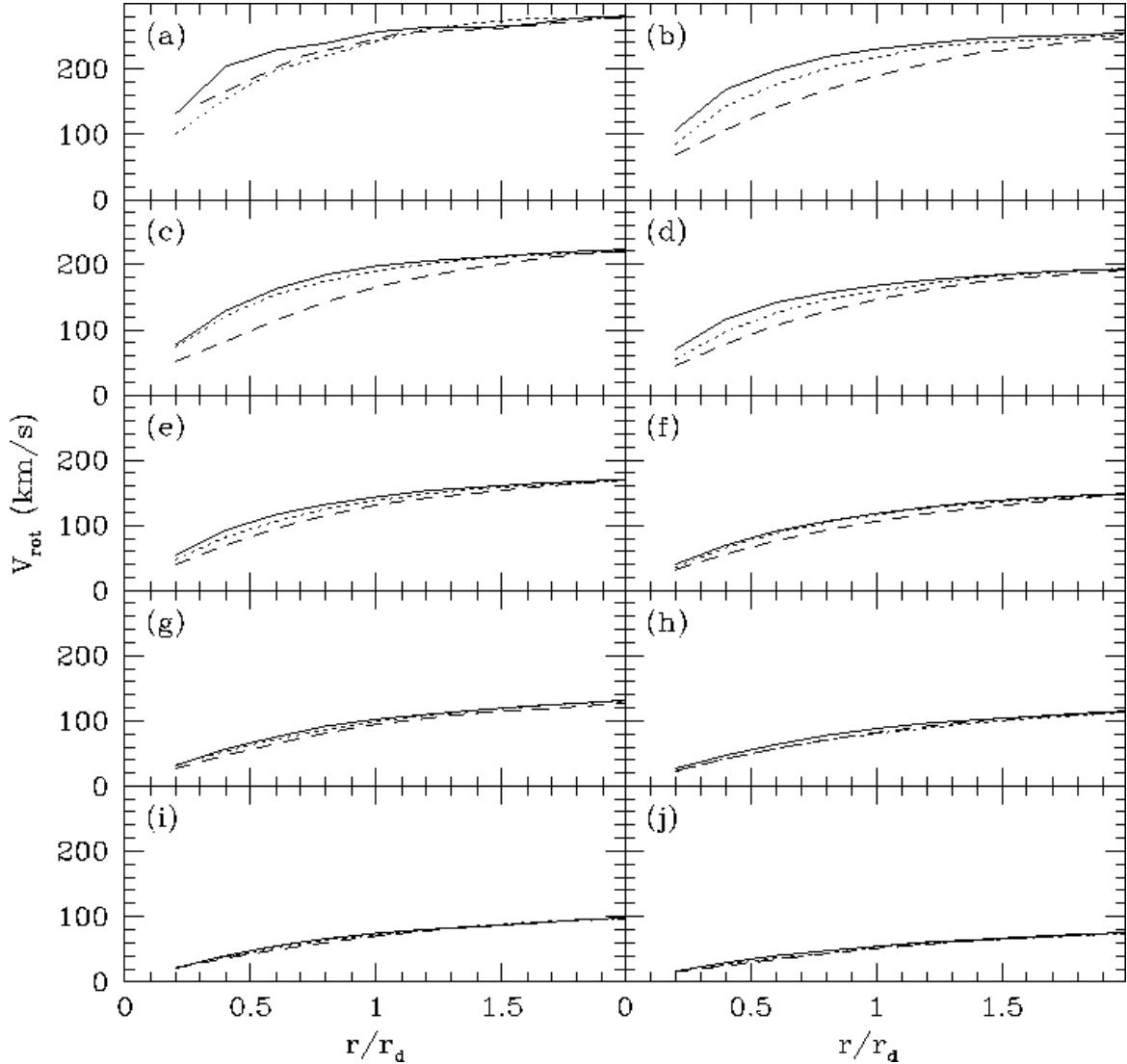


FIG. 10.— Template RCs divided into 3 inclination intervals:  $30^\circ \leq i < 70^\circ$  (solid lines),  $70^\circ \leq i < 80^\circ$  (dotted), and  $80^\circ \leq i \leq 90^\circ$  (dashed). Panels (a) through (j) correspond to the luminosity classes  $M_I = -23.8$  to  $-19.0$  in Table 1. Only the inner regions of the RCs are shown.

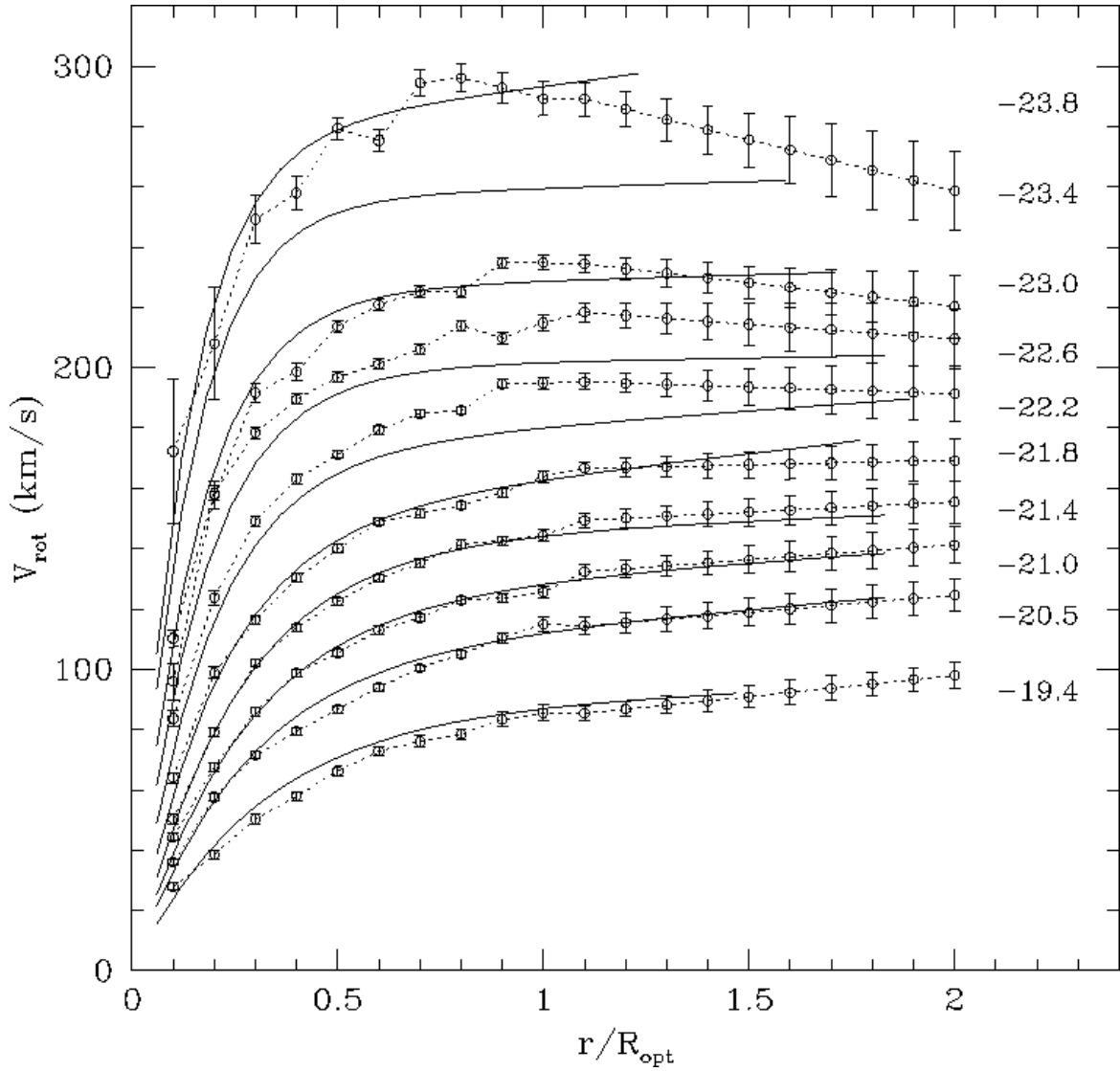


FIG. 11.—Polyex fits (solid lines) to the template RCs shown in Figure 4 are here compared to the average RCs obtained by PSS96 and kindly provided by Paolo Salucci. All PSS96 data points have been shifted by  $+10 \text{ km s}^{-1}$  to match the velocities of the template curves at  $R_{\text{opt}}$ .

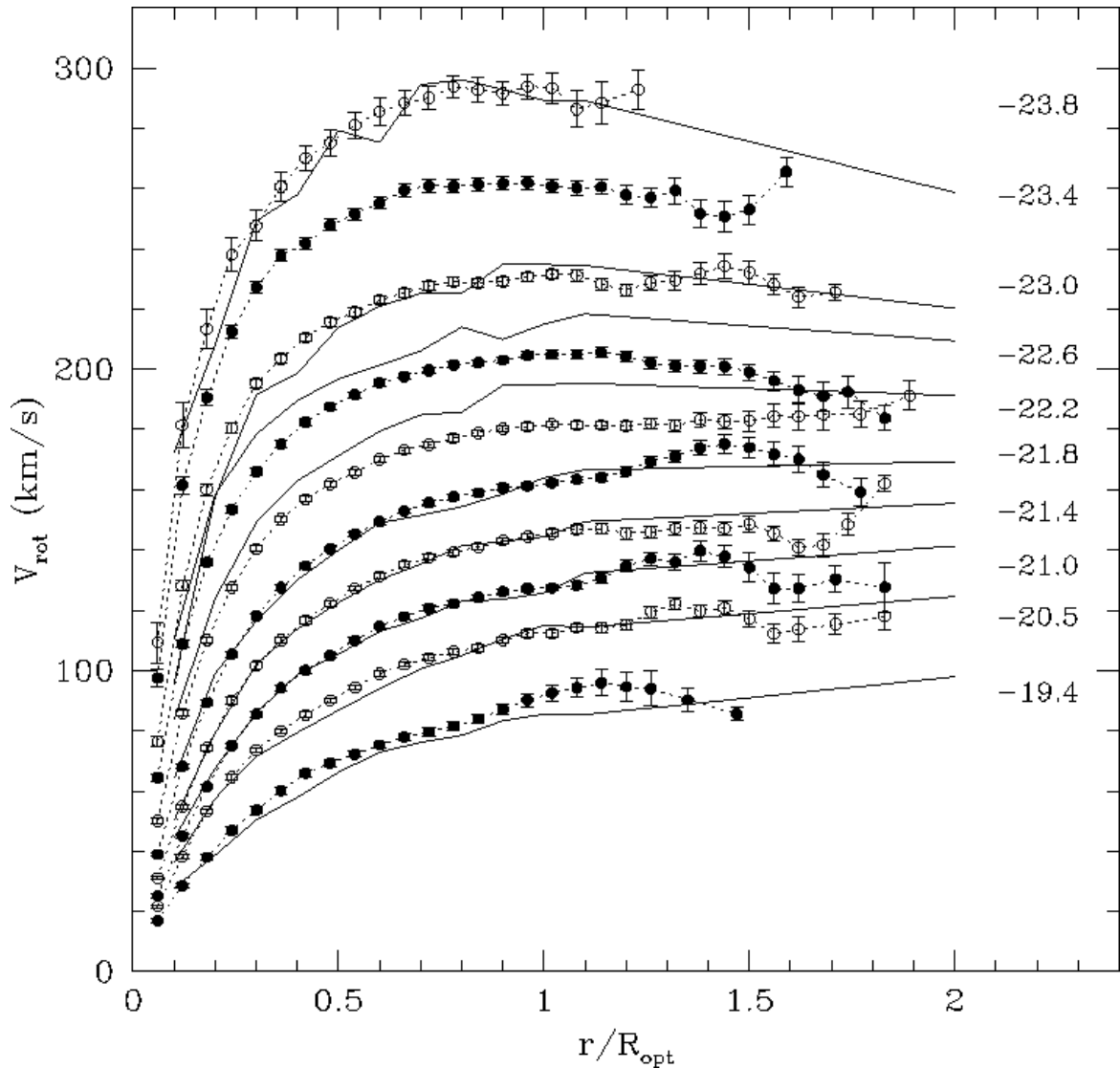


FIG. 12.— The URC tracings in Figure 11 are here reproduced as solid lines, superimposed on the  $R_{\text{opt}}$  template RC data from Figure 4.